THE JOURNAL OF PHYSICAL CHEMISTRY Letters

Letter

Cite This: J. Phys. Chem. Lett. 2018, 9, 6934−6940

pubs.acs.org/JPCL

Excitons and Biexciton Dynamics in Single $CsPbBr_3$ Perovskite Quantum Dots

Bin Li,[†,§,#] He Huang,[‡,#] Guofeng Zhang,*[,†,§] Changgang Yang,[†,§] Wenli Guo,[†,§] Ruiyun Chen,[†,§] Chengbing Qin,[†,§] Yan Gao,[†,§] Vasudevan P. Biju,[∥] Andrey L. Rogach,[‡] Liantuan Xiao,*[,†,§] and Suotang Jia[†,§]

[†]State Key Laboratory of Quantum Optics and Quantum Optics Devices, Institute of Laser Spectroscopy, Shanxi University, Taiyuan 030006, People's Republic of China

[‡]Department of Materials Science and Engineering, Centre for Functional Photonics (CFP), City University of Hong Kong, 83 Tat Chee Avenue, Kowloon, Hong Kong S.A.R.

[§]Collaborative Innovation Center of Extreme Optics, Shanxi University, Taiyuan 030006, People's Republic of China

[∥]Research Institute for Electronic Science, Hokkaido University, 001-0020 Sapporo, Japan

Supporting Information

ABSTRACT: Colloidal lead halide perovskite quantum dots, due to their optical versatility and facile solution processability, have been recently recognized as components of various optoelectronic devices. Detailed understanding of their exciton recombination dynamics at the single-particle level is necessary for utilizing their full potential. We conducted spectroscopic studies of the excitons and biexciton dynamics in single $CsPbBr_3$ perovskite quantum dots. It was found that while the rates of radiative recombination remain essentially constant, the overall relaxation process is dominated by nonradiative recombination of single excitons and biexcitons. The radiative lifetime scaling is determined to be ∼1.0 for single exciton and ∼4.4 for biexcitons. A linear dependence of fluorescence lifetime vs intensity distribution agrees well with the prediction of the model of multiple recombination centers. The blinking mechanism of $CsPbBr_3$ quantum dots is addressed by considering the trion states under higher excitation powers.

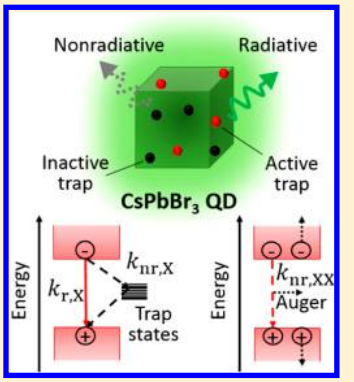

Lead halide perovskites are currently considered for a wide range of applications such as solar cells, light-emitting devices, and lasers because of their attractive optical and electronic properties combined with low cost and solution processability.[1−7] Among them, high-quality all-inorganic $CsPbX_3$ (X are Cl, Br, and/or I anions) perovskite quantum dots (QDs) have been fabricated via colloidal synthesis methods and exhibit useful optical properties such as high photoluminescence (PL), quantum yields (QYs), and tunable bandgaps covering entire visible spectrum.[8−10] Both efficient light-emitting devices and low-threshold lasing for all-inorganic perovskite QDs have been demonstrated recently.[11,12] In addition to the applications in conventional optoelectronic devices, perovskite QDs can be employed as single photon sources that might play a pivotal role in future quantum optical technologies.[13−15]

As perovskite QDs have a "soft" and predominantly ionic lattice, their optical and electronic properties are highly tolerant to structural defects and surface states.[16,17] However, for quite a number of cases, PLQYs of perovskite QDs still require improvements, as PLQYs are normally reported in the range of 50−95% in the green−red region and down to 10−20% in the blue.[17−19] The PLQY is determined by the competition between radiative and nonradiative recombination dynamics of photoexcited excitons.[20] The investigation of exciton recombination dynamics is of primary importance for diverse device applications because their efficiency and operating lifetime depend strongly on the nonradiative recombination process. In addition, blinking and irreversible photodegradation occur in perovskite QDs.[13,21−23] Blinking of $CsPbX_3$ perovskite QDs has been attributed to charging and discharging processes.[24] When the QD is charged to form a trion state, nonradiative Auger recombination of trion would compete with radiative recombination, resulting in a lower PLQY. The trion states are easier to be formed under higher excitation powers;[13] the lifetimes of trion states for perovskite QDs have been reported to be vastly different, such as ∼410 ps, ∼6 ns, and ∼33 ns.[14,15] Blinking has also been considered to be due to the activation and deactivation of multiple recombination centers (MRCs) in perovskite QDs.[21] MRCs refer to the short-lived traps (e.g., shallow traps) in perovskites;[25] their activation and deactivation modulate the nonradiative recombination rates and thus cause PL intensity jumps within a continuous distribution of emission states.[25−29] Systematic studies of the radiative and nonradiative recombi-

Received: October 8, 2018
Accepted: November 27, 2018
Published: November 28, 2018

DOI: 10.1021/acs.jpclett.8b03098
J. Phys. Chem. Lett. 2018, 9, 6934−6940

nation dynamics under different excitation powers to distinguish the different blinking mechanisms are highly necessary for utilizing the full potential of perovskite QDs in optoelectronic devices.

To understand the exciton recombination dynamics, it is also useful to investigate biexciton states of single perovskite QDs. A biexciton state can be created by absorbing two photons above QD's band gap or a single photon with higher energy that is greater than twice of the band gap.[30] The biexciton states can relax either radiatively or through the nonradiative Auger process.[30−32] For traditional core−shell CdSe-based QDs, the radiative lifetime scaling between biexciton states and single exciton states has been reported as approximately 4,[20,33,34] while the nonradiative Auger lifetime mainly depends on the shell thickness, crystal structure, and local nanoenvironment.[31,35,36] For $CsPbX_3$ perovskite QDs, their crystal and electronic structures are different from CdSe QDs,[37] and the radiative lifetime scaling for biexciton states still need to be determined. Besides, the biexciton QYs of $CsPbX_3$ perovskite QDs have been reported to be either quite low (~0.06)[13,14,24] or very high (>0.3),[38] meaning that systematic studies of the radiative and nonradiative recombination dynamics of biexcitons in single perovskite QDs are necessary.

In this study, we addressed in detail the radiative and nonradiative recombination dynamics of both single excitons and biexcitons in single $CsPbBr_3$ perovskite QDs under different excitation powers by using time-tagged, time-resolved, and time-correlated single-photon counting (TTTR-TCSPC). This technique provides ultimate flexibility in the data analysis,[39−42] to extract information about recombination dynamics of excitons from their PL trajectories, decays, and second-order correlation function ($g^{(2)}$) curves: the radiative/nonradiative rates, the PLQYs, the radiative lifetime scaling, and fluorescence lifetime intensity distributions (FLIDs) for the single excitons and biexcitons are obtained. On the basis of this information, we gained insights into the radiative and nonradiative recombination dynamics of single excitons and biexcitons, as well as blinking mechanisms of $CsPbBr_3$ perovskite QDs.

$CsPbBr_3$ perovskite QDs used in this work were synthesized by wet-chemical method, as presented in the Supporting Information (SI). Figure 1a shows the absorption and PL spectra of the QDs dispersed in toluene; the PL spectrum is centered at 515 nm with a full width at half-maximum of 20 nm. The solution PLQY has been measured to be over 50% at room temperature. Figure 1b shows the size histogram of the QDs with an average size (edge length of the cubic-shaped nanoparticles) of ~10 nm and a reasonable monodispersity, which was obtained from the transmission electron microscopy (TEM) images such as presented in the inset of Figure 1b, as well as in SI, Figure S1.

For the single-dot measurements, $CsPbBr_3$ perovskite QD solution in toluene has been mixed with polystyrene (1 wt %) and spin-coated onto a glass coverslip at a rotational speed of 3000 rpm. The QD areal density was kept below 0.1 μm^{-2} to allow us to observe single particles with a confocal microscope, such as shown in Figure 1c. It is worth noting that aggregates were also observed alongside with the single QDs; therefore, the latter had to be distinguished during the confocal scanning imaging process by a fast recognition method demonstrated in previous literature.[42] In addition, the $g^{(2)}$ as well as the time-gated $g^{(2)}$ as a more intuitive method[43] has been used to

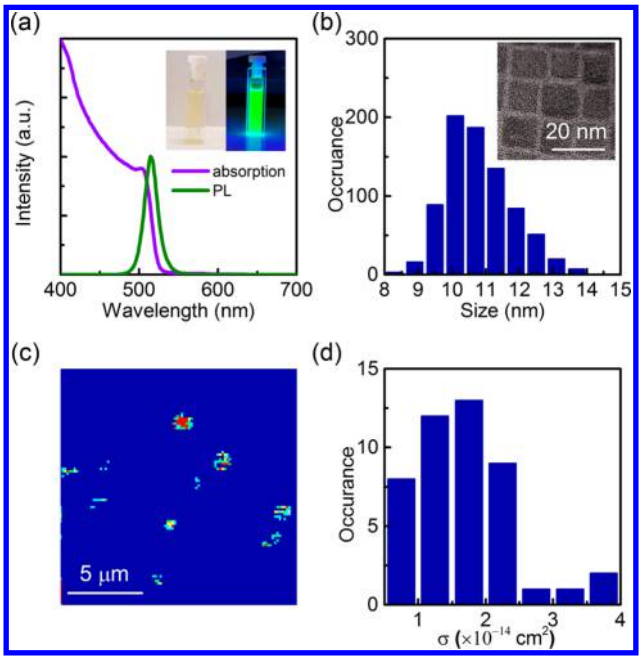

Figure 1. (a) Absorption and PL spectra of $CsPbBr_3$ QDs dispersed in toluene. Insets: photographs of the resultant solution under room and UV light. (b) Size histogram of $CsPbBr_3$ perovskite QDs. Inset: high-resolution transmission electron microscopy image. (c) Confocal scanning PL image of $CsPbBr_3$ perovskite QDs deposited on a glass substrate. (d) Histogram of the absorption cross sections (σ) of $CsPbBr_3$ perovskite QDs.

confirm that the investigated QDs are indeed single, isolated nanoparticles, as will be presented later. Using a home-built confocal fluorescence microscope setup (ref 44, see SI), the QDs in the polystyrene matrix deposited on the glass substrate were excited at 485 nm using a pulsed laser (90 ps pulse width, 10 MHz repetition rate). The emission from QDs was divided into two beams by using a beam splitter cube and detected using a pair of single-photon avalanche diode detectors and recorded using a TTTR-TCSPC data acquisition card with a temporal resolution of 16 ps. In the case of the pulsed excitation, the pump fluence $\langle N \rangle$ was evaluated as $\langle N \rangle = j_{exc}\sigma$, where j_{exc} is the per-pulse photon fluence and σ is the QD absorption cross section.[15,18,24] Detailed experimental methods for the determination of $\langle N \rangle$ and σ are provided in the SI; the distribution of σ for the $CsPbBr_3$ perovskite QDs is shown in Figure 1d. The average value of σ is 1.5×10^{-14} cm^2, which is consistent with the previous works.[15,18]

Figure 2a presents a typical PL intensity trajectory for single perovskite QDs obtained at $\langle N \rangle$ = 0.02 for the time frames from 0 to 100 s and from 310 to 345 s (see SI, Figure S2, for the whole PL trajectory from 0 to 450 s). The lifetime trajectory from 0 to 100 s in Figure 2a is obtained by monoexponential fitting of the PL decay curves which are extracted from photon streams at 0.5 s intervals. The lifetime values from 310 to 345 s in Figure 2a are obtained by fitting the PL decay curves of each intensity level with monoexponential functions. The corresponding $g^{(2)}$ curve with a low $g^2(0)$ value is shown in Figure 2b, indicating that the observed PL originates from a single QD. Figure 2c shows two typical PL decay curves obtained from two different PL regions marked in respective colors on Figure 2a. They were fitted by monoexponential functions with 4.5 ns (decay 1) and 8.9 ns (decay 2).

DOI: 10.1021/acs.jpclett.8b03098
J. Phys. Chem. Lett. 2018, 9, 6934−6940

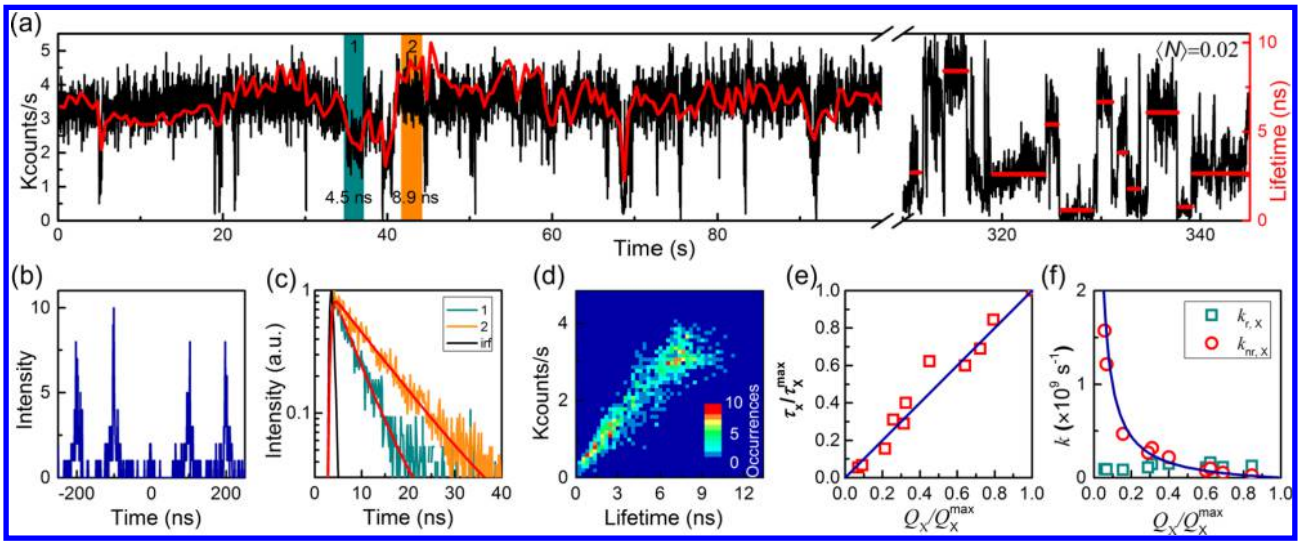

Figure 2. (a) PL intensity (black line) and lifetime (red line) trajectories for a single $CsPbBr_3$ QD, measured at $\langle N \rangle$ = 0.02 with time bin of 20 ms. (b) Corresponding second-order correlation function ($g^{(2)}$) of the single QD. (c) PL decay traces obtained from the PL regions marked by respective colors in (a). (d) Corresponding fluorescence lifetime-intensity distribution (FLID) in color scale; color changing from blue to red corresponds to increasing probability of occurrence of a given state in intensity-lifetime space. (e) PL lifetime plotted as a function of PLQYs derived from the PL trajectory of 310−345 s in (a), giving linear dependence with a slope of 1.01 ± 0.07. (f) Radiative and nonradiative rates of each PL intensity level as a function of the PLQY derived from the PL trajectory of 310−345 s in (a).

The corresponding FLID map obtained by monoexponential fitting of each time bin of 100 ms for the whole PL trajectory is shown in Figure 2d. The PL intensities approximately linearly correlated with lifetimes, which can be explained in the framework of the MRC model.[26−28] In this model, there are several nonradiative MRCs distributed in a QD.[25] The activation and deactivation of these MRCs modulate the nonradiative recombination rate $k_{nr,X}$ and thus cause multiple emission states in the PL intensity trajectory. The $k_{nr,X}$ is determined by the number of activated MRCs; when more MRCs are activated simultaneously, the $k_{nr,X}$ becomes higher, and the PL intensity as well as the lifetime would be further reduced. The MRC model can be used to explain the blinking phenomena, such as the linear correlation between the PL intensity and the lifetime as well as the low PLQYs of the off states, while these cannot be explained with the mechanisms involving Auger recombination (see SI for discussion).[45]

The PL trajectory from 310 to 345 s given in Figure 2a shows various intensity levels, which may be due to an increase in the number of nonradiative activated centers after the photoexcitation for 300 s (see the evolution of PL trajectory in Figure S2).[21,46,47] We define the maximal intensity level of the PL trajectory as the bright state, and all other lower intensity levels as the dim states (with various activated centers, according to MRC model). The PL decay curves from bright and dim states can be fitted with monoexponential functions. The bright state has the maximal PL lifetime, while the lifetimes of dim states reduce with PL intensities. The PL intensity level is proportional to the PLQY, and the PLQY at the highest intensity level is assumed to be unity.[32] Then, the PLQYs at other intensity levels can be calculated by $Q_X/Q_X^{max} = I_X/I_X^{max}$, where Q_X and I_X are the PLQY and intensity of dim states, respectively. By normalizing PLQYs and lifetimes with the maximal PLQY and lifetime, respectively, we plot τ_X/τ_X^{max} as a function of Q_X/Q_X^{max} as shown in Figure 2e, which can be fitted by a linear function with a slope of 1.01 ± 0.07. The slope of ∼1.0 represents the radiative lifetime scaling of single exciton (see SI, Figure S3, for statistical results). The value of ∼1.0 is far away from the radiative lifetime scaling between single exciton state and trion state, because the scaling of the trion state is equal to ∼2.0 which is a signature of exciton−trion blinking in the charging model.[20,28,34] On the basis of the PLQYs and lifetimes, the $k_{r,X}$ and $k_{nr,X}$ at various intensity levels can be calculated with $Q_X = k_{r,X}/(k_{r,X} + k_{nr,X})$, as shown in Figure 2f. We derived $k_{r,X}$ as 1.2×10^8 s^{-1}, while $k_{nr,X}$ changes with Q_X/Q_X^{max} and can be represented by

$$k_{nr,X} = k_{r,X} \times (Q_X^{-1} - 1) \quad (1)$$

As the $k_{nr,X}$ is an inverse proportional function of Q_X/Q_X^{max}, it will dominate the PLQY of excitons and the change of $k_{nr,X}$ results in the various PL intensity levels.[28] Thus, the observed linear dependence between the PL intensity and lifetime as shown in Figure 2e agrees well with the prediction of the MRC model.

Although trion states have been observed spectroscopically at cryogenic temperatures,[19,24,37] as well as by the femtosecond transient absorption at room temperature in previous works,[15,18] those results still could not unambiguously confirm the existence of trion states in $CsPbBr_3$ perovskite QDs. As the trion states are easier to be formed under higher excitation powers,[13,14] for the data we show in Figure 3a, the excitation power is increased to $\langle N \rangle$ = 0.2, and the blinking in the PL intensity trajectory becomes more frequent than that at $\langle N \rangle$ = 0.02. In Figure 3e, the PL intensity trajectory at $\langle N \rangle$ = 2 further evolves to bright−dim dual-state blinking, also called flickering (see the PL blinking with different time bins in SI, Figures S4 and S5). The corresponding $g^{(2)}$ curves as well as the time-gated $g^{(2)}$ curve are shown in parts b and f of Figure 3, respectively. The time-gated $g^{(2)}$ curve with a low $g^2(0)$ value indicates that PL photons originate from a single QD (for the method of time-gated $g^{(2)}$ analysis to recognize single QDs, see SI). In Figure 3c,g, we plot PL decay traces obtained from three different PL regions marked in respective colors in Figure 3a,e, respectively. At $\langle N \rangle$ = 0.2, as shown in Figure 3c, all three decay traces can still be fitted by monoexponential functions

DOI: 10.1021/acs.jpclett.8b03098
J. Phys. Chem. Lett. 2018, 9, 6934−6940

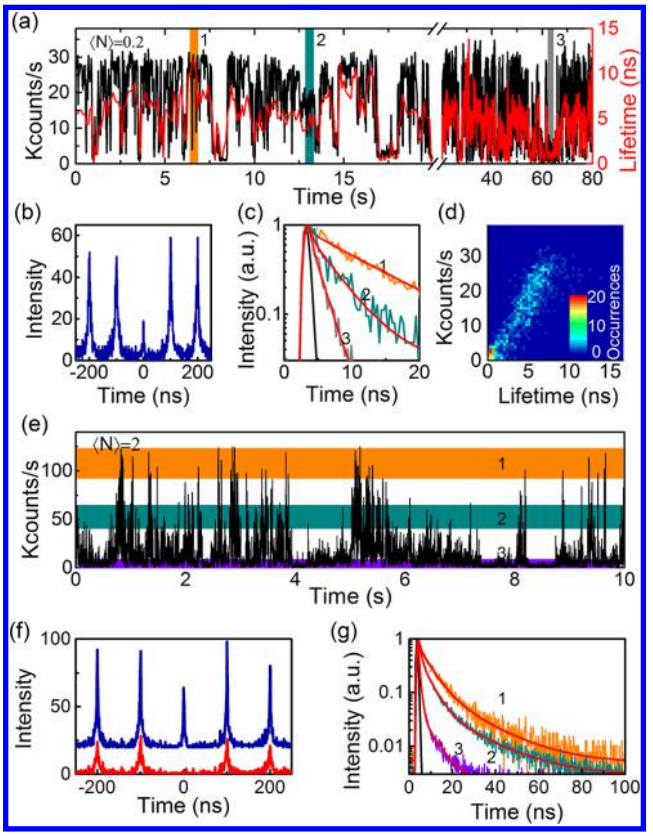

Figure 3. (a) PL intensity (black line) and lifetime (red line) trajectories for a single $CsPbBr_3$ QD measured at a higher excitation power of $\langle N \rangle = 0.2$. (b) Corresponding $g^{(2)}$ curve. (c) PL decay traces obtained from the PL regions marked by corresponding colors in (a). (d) Representation of FLID in the color scale obtained from the analysis of intensity and lifetime in (a). (e) PL intensity (black line) trajectory for a single $CsPbBr_3$ QD measured at $\langle N \rangle = 2$. (f) Corresponding $g^{(2)}$ curves. The blue and red curves are results of the original $g^{(2)}$ analysis and time-gated $g^{(2)}$ analysis with a threshold of 3.9 ns, respectively. (g) PL decay traces obtained by collecting emission in regions marked by corresponding colors in (e).

with 9.8 ns (decay 1), 4.1 ns (decay 2), and 1.7 ns (decay 3), respectively, which agrees with the prediction of the MRC model. At $\langle N \rangle = 2$ as shown in Figure 3g, all three PL decay traces can only be fitted by three-exponential functions (see the SI, Table S2, for the fitted results). For the decay trace of middle PL intensity region, it is found that the amplitude weight for one of the lifetimes (1.7 ns) is increased, which may mean more trion states in QD at higher excitation powers. Later on, in this article we will show that 1.7 ns is the lifetime of the trion state. In Figure 3d, the FLID map is presented from the analysis of intensity and lifetime data given in Figure 3a. It appears that FLID deviates slightly from the linear dependence, which may imply there are new recombination processes occur in perovskite QDs, such as trion states inducing Auger process.

We further investigated the radiative and nonradiative recombination dynamics of biexcitons. Under the weak excitation, the ratio of biexciton QYs (Q_{XX}) to single exciton QYs (Q_X) can be obtained as[31,32]

$$Q_{XX}/Q_X \approx g^{(2)}(0) \tag{2}$$

By using first-photon analysis[15,20,36,42] (see SI), the biexciton lifetime (τ_{XX}) can be obtained by fitting the decay trace with a monoexponential function as shown in Figure 4a. By measuring ~120 single QDs at $\langle N \rangle = 0.2$, the distribution of τ_{XX}/τ_X as a function of Q_{XX}/Q_X is shown in Figure 4b. When denoting the ratio between the radiative decay rates of biexcitons and single excitons as β, eq 2 can be rewritten as

$$Q_{XX}/Q_X = \beta \times \tau_{XX}/\tau_X \tag{3}$$

where β can be considered as the radiative lifetime scaling between single excitons and biexcitons. For the case of CdSe-based QDs, the value of β has been reported to be 4.0 according to the standard statistical scaling of radiative rates[20,31,33] but can also deviate from this value depending on the shell thickness for the core–shell particles.[35] We determined β value for the $CsPbBr_3$ perovskite QDs as 4.4 ± 1.5. The deviation of β from 4.0 may originate from specific size and shape of $CsPbBr_3$ QDs, as the size- and shape-dependent electronic structures of QDs dominate the radiative lifetimes of single excitons and biexcitons.[37,48]

The radiative and nonradiative Auger rates of biexcitons can be calculated by $k_{r,XX} = Q_{XX} \times k_{XX}$ and $k_{nr,XX} = (1 - Q_{XX}) \times k_{XX}$, respectively.[31,36] The Q_{XX} can be easily obtained from $g^{(2)}$ measurements with Q_X of ~50%, and the k_{XX} is the reciprocal of τ_{XX}. The $k_{r,XX}$ and $k_{nr,XX}$ values as a function of Q_{XX}/Q_X for ~120 QDs are plotted in Figure 4c. We have found that $k_{r,XX}$ remains almost similar for all the studied perovskite QDs with slightly different sizes, averaging at $\sim 3 \times 10^8\ s^{-1}$. $k_{nr,XX}$ changes with Q_{XX}/Q_X and can be represented by

$$k_{nr,XX} = k_{r,XX} \times (Q_{XX}^{-1} - 1) \tag{4}$$

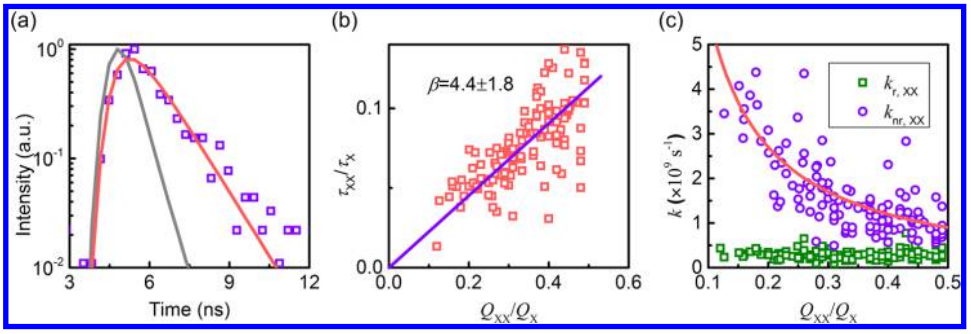

Figure 4. (a) Representative biexciton decay trace for a single $CsPbBr_3$ QD extracted from the two-channel TCSPC data. (b) Ratio of biexciton and single exciton lifetimes as a function of the ratio of their PLQYs derived from $g^{(2)}(0)$. (c) Radiative and nonradiative Auger rates of biexciton states as a function of the ratio of PLQYs of biexciton and single exciton states.

DOI: 10.1021/acs.jpclett.8b03098
J. Phys. Chem. Lett. 2018, 9, 6934–6940

As $k_{nr,XX}$ dominates Q_{XX}, the values of $k_{nr,XX}$ changing in the range of 1×10^9 to 4×10^9 s^{-1} (Figure 4c) leads to the changing Q_{XX}. For the CdSe-based core−shell QDs, $k_{nr,XX}$ can be influenced by the band gap energy, shape of the confining potential, carriers' wave function overlap, and their characteristic confinement width, which relates to the core size and shell thickness of QDs.[49] It has been reported that $k_{nr,XX}$ of perovskite QDs show a shallower volume dependence than the CdSe-based QDs.[50] However, the all-inorganic $CsPbBr_3$ perovskite QDs have a more pronounced volume-dependent $k_{nr,XX}$ than other perovskite QDs,[18,50] eventually due to the surface defect densities being greater or having a larger impact on Auger rate.[51] Therefore, the values of $k_{nr,XX}$ vary from dot to dot, which may be caused by the inhomogeneous size and shape of QDs as well as the heterogeneous surface defect density distribution. It also leads to the inhomogeneous Q_{XX} as observed here as well as reported in other studies.[13,14,24,38]

From the data of biexciton dynamics obtained above, we can deduce the lifetime of trions. Because the effective masses of electron and hole are nearly identical for $CsPbBr_3$ QDs,[37] the rates of negative and positive trions are similar. The radiative rate of trions can be estimated as $k_{r,X^*} = 2k_{r,X}$, where 2 is the radiative lifetime scaling between the trion and single exciton states.[20,33,34] The nonradiative rate of trions can be estimated as $k_{nr,X^*} = k_{nr,XX}/\beta$.[20,33] On the basis of these, the trion lifetime is estimated at 1.6 ns, which is close to the lifetime of 1.7 ns derived from the PL decay traces mentioned above. The trion lifetimes are dominated by the nonradiative Auger rates of trion states and may vary depending on perovskite QDs' sizes, compositions, and surface defect densities.[50] Therefore, the diversity of trion lifetimes reported in previous works[13−15] may be due to the different compositions and sizes and the heterogeneous surface defect densities.

Under higher excitation powers, biexciton state is easier to be created in a single QD after simultaneous absorption of two photons, and then one of the charge carriers in biexciton can be ejected out of the QD after receiving the biexciton Auger recombination energy,[30] so there are more trion states to be formed in $CsPbBr_3$ perovskite QDs. It has also been reported that the increase in the excitation power leads to increased fraction of time that the individual perovskite QD spends in the trion states.[13] The formation and annihilation of trion states are considered as the charging and discharging processes. On the basis of the above discussion, for $CsPbBr_3$ perovskite QDs, we conclude that the strong blinking (flickering) under higher excitation powers should be the result of the joint action of the activation and deactivation of MRCs and the charging and discharging processes.

A summary table of photophysical parameters for single $CsPbBr_3$ QDs obtained in this work is presented in SI, Table S2. From results of this work, the surface trap states are found to play a crucial role in the PLQYs, the blinking behavior, and the excitons and biexciton dynamics of the $CsPbBr_3$ QDs. It has been previously reported that through proper ligand passivation of surface, the PLQYs could be raised close to ∼100%, and the trion generation under weak photoexcitation could be suppressed.[52−54] We note that a linear dependence of FLID has been previously observed for $CsPbI_3$ QDs,[21] indicating that the MRC model can be suitable too to describe their blinking dynamics (see SI for related comments).

In summary, we have investigated the excitons and biexciton dynamics in single $CsPbBr_3$ perovskite QDs by using TTTR-TCSPC technique. The radiative/nonradiative rates, the PLQYs, the radiative lifetime scaling, and the FLIDs for single exciton and biexcitons have been obtained. The data show that while the rates of radiative recombination remain essentially constant, the overall relaxation process is dominated by nonradiative recombination of single excitons and biexcitons. The radiative lifetime scaling of single excitons has been determined to be ∼1.0 according to the relationship of PL lifetimes and QYs. The radiative lifetime scaling of biexcitons has been estimated to be ∼4.4. The linear dependence of FLID indicates that the activation and deactivation of MRCs dominate the blinking under lower excitation powers. Under higher excitation powers, the blinking originates from joint action of the activation and deactivation of MRCs and the charging and discharging processes. Proper surface passivation techniques have been used to suppress the PL blinking and improve the PLQYs of perovskite QDs.

■ ASSOCIATED CONTENT

Supporting Information

The Supporting Information is available free of charge on the ACS Publications website at DOI: 10.1021/acs.jpclett.8b03098.

Sample preparation and characterizations, experimental setup, estimation of $\langle N \rangle$ and calculation of the absorption cross section, method for obtaining biexciton lifetimes, method for the time-gated $g^{(2)}$, and comparison between MRC and DCET models (PDF)

■ AUTHOR INFORMATION

Corresponding Authors

*E-mail: guofeng.zhang@sxu.edu.cn (G.Z.).
*E-mail: xlt@sxu.edu.cn (L. X.).

ORCID

Bin Li: 0000-0002-5817-6792
He Huang: 0000-0002-2052-718X
Guofeng Zhang: 0000-0002-9030-0431
Chengbing Qin: 0000-0002-6822-5113
Vasudevan P. Biju: 0000-0003-3650-9637
Andrey L. Rogach: 0000-0002-8263-8141

Author Contributions

#Equal contribution.

Notes

The authors declare no competing financial interest.

■ ACKNOWLEDGMENTS

We acknowledge financial support from the National Key R&D Program of China (no. 2017YFA0304203), Natural Science Foundation of China (nos. 61527824, 61675119, U1510133, 11434007, 11504216, 61605104), Research Grant Council of Hong Kong S.A.R. (GRF project CityU 11337616), Program for Changjiang Scholars and Innovative Research Team (no. IRT13076), 1331 Key Subjects Construction, and 111 project (grant no. D18001).

■ REFERENCES

(1) Chen, H.; Ye, F.; Tang, W. T.; He, J. J.; Yin, M. S.; Wang, Y. B.; Xie, F. X.; Bi, E. B.; Yang, X. D.; Gratzel, M.; Han, L. A Solvent- and Vacuum-Free Route to Large-Area Perovskite Films for Efficient Solar Modules. *Nature* **2017**, *550*, 92−95.

(2) Yang, W. S.; Park, B. W.; Jung, E. H.; Jeon, N. J.; Kim, Y. C.; Lee, D. U.; Shin, S. S.; Seo, J.; Kim, E. K.; Noh, J. H.; et al. Iodide

DOI: 10.1021/acs.jpclett.8b03098
J. Phys. Chem. Lett. 2018, 9, 6934−6940

Management in Formamidinium-Lead-Halide-Based Perovskite Layers for Efficient Solar Cells. *Science* **2017**, *356*, 1376−1379.
(3) Tang, B.; Dong, H. X.; Sun, L. X.; Zheng, W. H.; Wang, Q.; Sun, F. F.; Jiang, X. W.; Pan, A. L.; Zhang, L. Single-Mode Lasers Based on Cesium Lead Halide Perovskite Submicron Spheres. *ACS Nano* **2017**, *11*, 10681−10688.
(4) Debroye, E.; Yuan, H.; Bladt, E.; Baekelant, W.; Van der Auweraer, M.; Hofkens, J.; Bals, S.; Roeffaers, M. B. J. Facile Morphology-Controlled Synthesis of Organolead Iodide Perovskite Nanocrystals Using Binary Capping Agents. *ChemNanoMat* **2017**, *3*, 223−227.
(5) Yuyama, K.-I.; Islam, M. J.; Takahashi, K.; Nakamura, T.; Biju, V. Crystallization of Methylammonium Lead Halide Perovskites by Optical Trapping. *Angew. Chem., Int. Ed.* **2018**, *57*, 13424.
(6) Liu, X.; Yu, D.; Huo, C.; Song, X.; Gao, Y.; Zhang, S.; Zeng, H. A. Perovskite Light-Emitting Device Driven by Low-Frequency Alternating Current Voltage. *Adv. Opt. Mater.* **2018**, *6*, 1800206.
(7) Schmidt, L. C.; Pertegás, A.; González-Carrero, S.; Malinkiewicz, O.; Agouram, S.; Mínguez Espallargas, G.; Bolink, H. J.; Galian, R. E.; Pérez-Prieto, J. Nontemplate Synthesis of $CH_3NH_3PbBr_3$ Perovskite Nanoparticles. *J. Am. Chem. Soc.* **2014**, *136*, 850−853.
(8) Zhang, F.; Zhong, H.; Chen, C.; Wu, X.-g.; Hu, X.; Huang, H.; Han, J.; Zou, B.; Dong, Y. Brightly Luminescent and Color-Tunable Colloidal $CH_3NH_3PbX_3$ (X = Br, I, Cl) Quantum Dots: Potential Alternatives for Display Technology. *ACS Nano* **2015**, *9*, 4533−4542.
(9) Huang, H.; Polavarapu, L.; Sichert, J. A.; Susha, A. S.; Urban, A. S.; Rogach, A. L. Colloidal Lead Halide Perovskite Nanocrystals: Synthesis, Optical Properties and Applications. *NPG Asia Mater.* **2016**, *8*, e328.
(10) Ravi, V. K.; Markad, G. B.; Nag, A. Band Edge Energies and Excitonic Transition Probabilities of Colloidal $CsPbX_3$ (X = Cl, Br, I) Perovskite Nanocrystals. *ACS Energy Lett.* **2016**, *1*, 665−671.
(11) Chiba, T.; Hoshi, K.; Pu, Y. J.; Takeda, Y.; Hayashi, Y.; Ohisa, S.; Kawata, S.; Kido, J. High-Efficiency Perovskite Quantum-Dot Light-Emitting Devices by Effective Washing Process and Interfacial Energy Level Alignment. *ACS Appl. Mater. Interfaces* **2017**, *9*, 18054−18060.
(12) Yakunin, S.; Protesescu, L.; Krieg, F.; Bodnarchuk, M. I.; Nedelcu, G.; Humer, M.; De Luca, G.; Fiebig, M.; Heiss, W.; Kovalenko, M. V. Low-Threshold Amplified Spontaneous Emission and Lasing from Colloidal Nanocrystals of Caesium Lead Halide Perovskites. *Nat. Commun.* **2015**, *6*, 8056.
(13) Park, Y. S.; Guo, S. J.; Makarov, N. S.; Klimov, V. I. Room Temperature Single-Photon Emission from Individual Perovskite Quantum Dots. *ACS Nano* **2015**, *9*, 10386−10393.
(14) Hu, F. R.; Yin, C. Y.; Zhang, H. C.; Sun, C.; Yu, W. W.; Zhang, C. F.; Wang, X. Y.; Zhang, Y.; Xiao, M. Slow Auger Recombination of Charged Excitons in Nonblinking Perovskite Nanocrystals without Spectral Diffusion. *Nano Lett.* **2016**, *16*, 6425−6430.
(15) Yarita, N.; Tahara, H.; Ihara, T.; Kawawaki, T.; Sato, R.; Saruyama, M.; Teranishi, T.; Kanemitsu, Y. Dynamics of Charged Excitons and Biexcitons in $CsPbBr_3$ Perovskite Nanocrystals Revealed by Femtosecond Transient-Absorption and Single-Dot Luminescence Spectroscopy. *J. Phys. Chem. Lett.* **2017**, *8*, 1413−1418.
(16) Huang, H.; Bodnarchuk, M. I.; Kershaw, S. V.; Kovalenko, M. V.; Rogach, A. L. Lead Halide Perovskite Nanocrystals in the Research Spotlight: Stability and Defect Tolerance. *ACS Energy Lett.* **2017**, *2*, 2071−2083.
(17) Akkerman, Q. A.; Raino, G.; Kovalenko, M. V.; Manna, L. Genesis, Challenges and Opportunities for Colloidal Lead Halide Perovskite Nanocrystals. *Nat. Mater.* **2018**, *17*, 394−405.
(18) Makarov, N. S.; Guo, S. J.; Isaienko, O.; Liu, W. Y.; Robel, I.; Klimov, V. I. Spectral and Dynamical Properties of Single Excitons, Biexcitons, and Trions in Cesium-Lead-Halide Perovskite Quantum Dots. *Nano Lett.* **2016**, *16*, 2349−2362.
(19) Fu, M.; Tamarat, P.; Huang, H.; Even, J.; Rogach, A. L.; Lounis, B. Neutral and Charged Exciton Fine Structure in Single Lead Halide Perovskite Nanocrystals Revealed by Magneto-Optical Spectroscopy. *Nano Lett.* **2017**, *17*, 2895−2901.
(20) Park, Y. S.; Bae, W. K.; Pietryga, J. M.; Klimov, V. I. Auger Recombination of Biexcitons and Negative and Positive Trions in Individual Quantum Dots. *ACS Nano* **2014**, *8*, 7288−7296.
(21) Yuan, G.; Ritchie, C.; Ritter, M.; Murphy, S.; Gómez, D. E.; Mulvaney, P. The Degradation and Blinking of Single $CsPbI_3$ Perovskite Quantum Dots. *J. Phys. Chem. C* **2018**, *122*, 13407−13415.
(22) Yuan, H.; Debroye, E.; Caliandro, G.; Janssen, K. P.; van Loon, J.; Kirschhock, C. E.; Martens, J. A.; Hofkens, J.; Roeffaers, M. B. Photoluminescence Blinking of Single-Crystal Methylammonium Lead Iodide Perovskite Nanorods Induced by Surface Traps. *ACS Omega* **2016**, *1*, 148−159.
(23) Yuan, H.; Debroye, E.; Janssen, K.; Naiki, H.; Steuwe, C.; Lu, G.; Moris, M.; Orgiu, E.; Uji-i, H.; De Schryver, F.; et al. Degradation of Methylammonium Lead Iodide Perovskite Structures through Light and Electron Beam Driven Ion Migration. *J. Phys. Chem. Lett.* **2016**, *7*, 561−566.
(24) Hu, F. R.; Zhang, H. C.; Sun, C.; Yin, C. Y.; Lv, B. H.; Zhang, C. F.; Yu, W. W.; Wang, X. Y.; Zhang, Y.; Xiao, M. Superior Optical Properties of Perovskite Nanocrystals as Single Photon Emitters. *ACS Nano* **2015**, *9*, 12410−12416.
(25) Tachikawa, T.; Karimata, I.; Kobori, Y. Surface Charge Trapping in Organolead Halide Perovskites Explored by Single-Particle Photoluminescence Imaging. *J. Phys. Chem. Lett.* **2015**, *6*, 3195−3201.
(26) Frantsuzov, P. A.; Volkan-Kacso, S.; Janko, B. Model of Fluorescence Intermittency of Single Colloidal Semiconductor Quantum Dots Using Multiple Recombination Centers. *Phys. Rev. Lett.* **2009**, *103*, 207402.
(27) Cordones, A. A.; Leone, S. R. Mechanisms for Charge Trapping in Single Semiconductor Nanocrystals Probed by Fluorescence Blinking. *Chem. Soc. Rev.* **2013**, *42*, 3209−3221.
(28) Yuan, G.; Gómez, D. E.; Kirkwood, N.; Boldt, K.; Mulvaney, P. Two Mechanisms Determine Quantum Dot Blinking. *ACS Nano* **2018**, *12*, 3397−3405.
(29) Yuan, H.; Debroye, E.; Bladt, E.; Lu, G.; Keshavarz, M.; Janssen, K. P. F.; Roeffaers, M. B. J.; Bals, S.; Sargent, E. H.; Hofkens, J. Imaging Heterogeneously Distributed Photo-Active Traps in Perovskite Single Crystals. *Adv. Mater.* **2018**, *30*, 1705494.
(30) Hu, F. R.; Lv, B. H.; Yin, C. Y.; Zhang, C. F.; Wang, X. Y.; Lounis, B.; Xiao, M. Carrier Multiplication in a Single Semiconductor Nanocrystal. *Phys. Rev. Lett.* **2016**, *116*, 106404.
(31) Li, Z. J.; Zhang, G. F.; Li, B.; Chen, R. Y.; Qin, C. B.; Gao, Y.; Xiao, L. T.; Jia, S. T. Enhanced Biexciton Emission from Single Quantum Dots Encased in N-Type Semiconductor Nanoparticles. *Appl. Phys. Lett.* **2017**, *111*, 153106.
(32) Nair, G.; Zhao, J.; Bawendi, M. G. Biexciton Quantum Yield of Single Semiconductor Nanocrystals from Photon Statistics. *Nano Lett.* **2011**, *11*, 1136−1140.
(33) Klimov, V. I. Multicarrier Interactions in Semiconductor Nanocrystals in Relation to the Phenomena of Auger Recombination and Carrier Multiplication. *Annu. Rev. Condens. Matter Phys.* **2014**, *5*, 285−316.
(34) Sampat, S.; Karan, N. S.; Guo, T.; Htoon, H.; Hollingsworth, J. A.; Malko, A. V. Multistate Blinking and Scaling of Recombination Rates in Individual Silica-Coated CdSe/CdS Nanocrystals. *ACS Photonics* **2015**, *2*, 1505−1512.
(35) Hiroshige, N.; Ihara, T.; Saruyama, M.; Teranishi, T.; Kanemitsu, Y. Coulomb-Enhanced Radiative Recombination of Biexcitons in Single Giant-Shell CdSe/CdS Core/Shell Nanocrystals. *J. Phys. Chem. Lett.* **2017**, *8*, 1961−1966.
(36) Park, Y. S.; Bae, W. K.; Padilha, L. A.; Pietryga, J. M.; Klimov, V. I. Effect of the Core/Shell Interface on Auger Recombination Evaluated by Single-Quantum-Dot Spectroscopy. *Nano Lett.* **2014**, *14*, 396−402.
(37) Becker, M. A.; Vaxenburg, R.; Nedelcu, G.; Sercel, P. C.; Shabaev, A.; Mehl, M. J.; Michopoulos, J. G.; Lambrakos, S. G.; Bernstein, N.; Lyons, J. L.; et al. Bright Triplet Excitons in Caesium Lead Halide Perovskites. *Nature* **2018**, *553*, 189−193.

DOI: 10.1021/acs.jpclett.8b03098
J. Phys. Chem. Lett. 2018, 9, 6934−6940

(38) Raino, G.; Nedelcu, G.; Protesescu, L.; Bodnarchuk, M. I.; Kovalenko, M. V.; Mahrt, R. F.; Stoferle, T. Single Cesium Lead Halide Perovskite Nanocrystals at Low Temperature: Fast Single Photon Emission, Reduced Blinking, and Exciton Fine Structure. *ACS Nano* **2016**, *10*, 2485−2490.
(39) Zhang, G.; Xiao, L.; Chen, R.; Gao, Y.; Wang, X.; Jia, S. Single-Molecule Interfacial Electron Transfer Dynamics Manipulated by an External Electric Current. *Phys. Chem. Chem. Phys.* **2011**, *13*, 13815−12820.
(40) Zhang, G.; Xiao, L.; Zhang, F.; Wang, X.; Jia, S. Single Molecules Reorientation Reveals the Dynamics of Polymer Glasses Surface. *Phys. Chem. Chem. Phys.* **2010**, *12*, 2308−2312.
(41) Yang, C. G.; Zhang, G. F.; Feng, L. H.; Li, B.; Li, Z. J.; Chen, R. Y.; Qin, C. B.; Gao, Y.; Xiao, L. T.; Jia, S. T. Suppressing the Photobleaching and Photoluminescence Intermittency of Single Near-Infrared CdSeTe/ZnS Quantum Dots with p-Phenylenediamine. *Opt. Express* **2018**, *26*, 11889−11902.
(42) Li, B.; Zhang, G. F.; Yang, C. G.; Li, Z. J.; Chen, R. Y.; Qin, C. B.; Gao, Y.; Huang, H.; Xiao, L. T.; Jia, S. T. Fast Recognition of Single Quantum Dots from High Multi-Exciton Emission and Clustering Effects. *Opt. Express* **2018**, *26*, 4674−4685.
(43) Mangum, B. D.; Ghosh, Y.; Hollingsworth, J. A.; Htoon, H. Disentangling the Effects of Clustering and Multi-Exciton Emission in Second-Order Photon Correlation Experiments. *Opt. Express* **2013**, *21*, 7419−7426.
(44) Li, B.; Zhang, G. F.; Wang, Z.; Li, Z. J.; Chen, R. Y.; Qin, C. B.; Gao, Y.; Xiao, L. T.; Jia, S. T. Suppressing the Fluorescence Blinking of Single Quantum Dots Encased in N-Type Semiconductor Nanoparticles. *Sci. Rep.* **2016**, *6*, 32662.
(45) Gibson, N. A.; Koscher, B. A.; Alivisatos, A. P.; Leone, S. R. Excitation Intensity Dependence of Photoluminescence Blinking in $CsPbBr_3$ Perovskite Nanocrystals. *J. Phys. Chem. C* **2018**, *122*, 12106−12113.
(46) Yamashita, S. I.; Hamada, M.; Nakanishi, S.; Saito, H.; Nosaka, Y.; Wakida, S. I.; Biju, V. Auger Ionization Beats Photo-Oxidation of Semiconductor Quantum Dots: Extended Stability of Single-Molecule Photoluminescence. *Angew. Chem., Int. Ed.* **2015**, *54*, 3892−3896.
(47) Thomas, E. M.; Ghimire, S.; Kohara, R.; Anil, A. N.; Yuyama, K.-I.; Takano, Y.; Thomas, K. G.; Biju, V. Blinking Suppression in Highly Excited CdSe/ZnS Quantum Dots by Electron Transfer under Large Positive Gibbs (Free) Energy Change. *ACS Nano* **2018**, *12*, 9060−9069.
(48) Huang, X. N.; Xu, Q. F.; Zhang, C. F.; Wang, X. Y.; Xiao, M. Energy Transfer of Biexcitons in a Single Semiconductor Nanocrystal. *Nano Lett.* **2016**, *16*, 2492−2496.
(49) Vaxenburg, R.; Rodina, A.; Lifshitz, E.; Efros, A. L. Biexciton Auger Recombination in CdSe/CdS Core/Shell Semiconductor Nanocrystals. *Nano Lett.* **2016**, *16*, 2503−2511.
(50) Eperon, G. E.; Jedlicka, E.; Ginger, D. S. Biexciton Auger Recombination Differs in Hybrid and Inorganic Halide Perovskite Quantum Dots. *J. Phys. Chem. Lett.* **2018**, *9*, 104−109.
(51) Johnston, M. B.; Herz, L. M. Hybrid Perovskites for Photovoltaics: Charge-Carrier Recombination, Diffusion, and Radiative Efficiencies. *Acc. Chem. Res.* **2016**, *49*, 146−154.
(52) Koscher, B. A.; Swabeck, J. K.; Bronstein, N. D.; Alivisatos, A. P. Essentially Trap-Free $CsPbBr_3$ Colloidal Nanocrystals by Postsynthetic Thiocyanate Surface Treatment. *J. Am. Chem. Soc.* **2017**, *139*, 6566−6569.
(53) Liu, F.; Zhang, Y.; Ding, C.; Kobayashi, S.; Izuishi, T.; Nakazawa, N.; Toyoda, T.; Ohta, T.; Hayase, S.; Minemoto, T.; et al. Highly Luminescent Phase-Stable $CsPbI_3$ Perovskite Quantum Dots Achieving Near 100% Absolute Photoluminescence Quantum Yield. *ACS Nano* **2017**, *11*, 10373−10383.
(54) Nakahara, S.; Tahara, H.; Yumoto, G.; Kawawaki, T.; Saruyama, M.; Sato, R.; Teranishi, T.; Kanemitsu, Y. Suppression of Trion Formation in $CsPbBr_3$ Perovskite Nanocrystals by Postsynthetic Surface Modification. *J. Phys. Chem. C* **2018**, *122*, 22188−22193.

DOI: 10.1021/acs.jpclett.8b03098
J. Phys. Chem. Lett. 2018, 9, 6934−6940